Earth and Planetary Science Letters 531 (2020) 116009

Contents lists available at ScienceDirect

Earth and Planetary Science Letters

www.elsevier.com/locate/epsl

Chemical compositions of the outer core examined by first principles calculations

Koichiro Umemoto [a,*], Kei Hirose [a,b]

[a] Earth-Life Science Institute, Tokyo Institute of Technology, Meguro, Tokyo 150-8550, Japan
[b] Department of Earth and Planetary Science, The University of Tokyo, Bunkyo, Tokyo 113-0033, Japan

ARTICLE INFO

Article history:
Received 1 May 2019
Received in revised form 17 November 2019
Accepted 3 December 2019
Available online 10 December 2019
Editor: B. Buffett

Keywords:
outer core
chemical composition
liquid under high pressure
first principles

ABSTRACT

We have examined the density and bulk sound velocity of liquid iron alloys, $(Fe, Ni)_X(H, Si, O, S, C)_{1-X}$, at Earth's outer core pressure and temperature conditions based on first-principles molecular dynamics simulations. The nonideal mixing effects on volume and velocity were found to be negligible for all combinations of different liquid alloys examined. By comparing the results with seismological observations, we searched for possible chemical compositions for the outer core. Hydrogen is found to be a primary light element when the inner-core boundary temperature T_{ICB} is 4,800 K to 5,400 K. If this is the case, it is suggested that a large amount of water was delivered to the Earth during its accretionary stage and that the present-day core temperature is relatively low. On the other hand, oxygen is the most important light element if $T_{ICB} = 6{,}000$ K, consistent with the previous calculations by Badro et al. (2014) at $T_{ICB} = 6{,}300$ K. To further constrain the chemical composition of the outer core, it is necessary to take into account other constraints besides its density and bulk sound velocity; melting temperature, simultaneous solubilities of multiple of light elements, and so forth.

1. Introduction

The chemical composition of the Earth's liquid outer core still remains unknown (see reviews by Poirier, 1994; Hirose et al., 2013; Li and Fei, 2014). The Preliminary Reference Earth Model (PREM) deduced from seismology (Dziewonski and Anderson, 1981) suggests that the density and the bulk sound velocity of the outer core is ~10% lower and ~5% faster than those of liquid pure iron, respectively (e.g., Anderson and Ahrens, 1994; Dewaele et al., 2006; Ichikawa et al., 2014; Wagle and Steinle-Neumann, 2019). These differences indicate that the outer core includes substantial amounts of light elements such as silicon, oxygen, sulfur, carbon, and hydrogen, in addition to iron and nickel. In order to constrain the chemical composition of the outer core that is compatible with seismic observations, previous first-principles computational studies calculated the densities and bulk sound velocities of liquid iron (Alfé et al., 2002; Vočadlo et al., 2003; Ichikawa et al., 2014; Wagle and Steinle-Neumann, 2019) and alloys (Alfé et al., 2007; Badro et al., 2014; Umemoto et al., 2014; Umemoto and Hirose, 2015) under Earth's core conditions. Recent high-pressure experimental studies also reported the density (Morard et al., 2013, 2017) and velocity (Nakajima et al., 2015; Kawaguchi et al., 2017) of liquid iron alloys to 94 GPa, which is still lower than the core pressure range (>135 GPa).

The calculations by Badro et al. (2014) searched for the possible liquid core compositions in Fe-Si-O-S-C that account for the outer core density deficit and velocity excess with respect to pure iron at core-mantle boundary (CMB) and inner core boundary (ICB) conditions, and argued that oxygen is an important core light element. However, they did not consider the effect of hydrogen. Recent planet formation theories suggest that an extensive amount of water may have been brought to the Earth in its accretion stage (e.g., Walsh et al., 2011; Sato et al., 2016). And, hydrogen is highly siderophile under pressure (Okuchi, 1997; Shibazaki et al., 2009; Pépin et al., 2014; Iizuka-Oku et al., 2017). This has been challenged by the metal-silicate partitioning experiments by Clesi et al. (2018) and Malavergne et al. (2019). However, their claims were based on the presence of minor amounts of hydrogen in metal at 1 bar. It is known that the solubility of hydrogen in solid Fe is very low at ambient condition; $H/Fe < 10^{-5}$ (Fukai and Suzuki, 1986). Most of the hydrogen atoms escapes from solid iron during decompression (Okuchi, 1997; Iizuka-Oku et al., 2017). The experiments performed by Okuchi (1997) demonstrated that more than 95% of H_2O in a magma ocean could have been incorporated into core-forming metals. Our previous calculations have shown that liquid iron alloyed with 1.0 wt% H reconciles both the density and the

* Corresponding author.
E-mail address: umemoto@elsi.jp (K. Umemoto).

https://doi.org/10.1016/j.epsl.2019.116009
0012-821X/

sound velocity observed in the outer core (Umemoto and Hirose, 2015).

We report here the results of first-principles molecular dynamics on binary liquid iron alloys containing silicon, oxygen, sulfur, carbon, and hydrogen at outer core conditions. Nonideal mixing effect is also examined in ternary and quaternary alloy systems. Using them, we estimate the density and bulk sound velocity of liquid iron alloyed with multiple light elements along geotherms and compare them with the PREM profiles to constrain the chemical composition of the outer core.

2. Computational method

We performed first-principles molecular dynamics (FPMD) calculations using pseudopotentials within the density-functional theory with 128 atoms in fixed cubic cells corresponding to ~100–350 GPa. The procedures of FPMD for these liquid alloys were the same as in our previous study (Umemoto and Hirose, 2015). We performed FPMD at 10,000 K for 2 picoseconds to obtain a liquid structure, which was confirmed from radial distribution function and mean square displacements. Then, the cell was quenched to a target temperature (4,000 to 7,000 K) and allowed to equilibrate for 2 picoseconds. Finally, FPMD was performed for 10 picoseconds or longer to calculate pressure and energy by taking their averages over time. The temperature was controlled using a Nosé-Hoover thermostat (Nosé, 1984; Hoover, 1985). Time steps were 1 (or 2) femtosecond at 10,000 K for generating a liquid structure, and 0.5 (or 1) femtosecond at target temperature where pressure and energy were calculated for Fe alloys containing hydrogen (or without hydrogen). The pseudopotentials for all atomic species were generated using Vanderbilt's method (Vanderbilt, 1990). A Perdew-Burke-Ernzerhof (PBE)-type generalized-gradient approximation (GGA) functional was used for exchange-correlation (XC) potential (Perdew et al., 1996). The electronic configurations for pseudopotential generation were $3s^2 3p^6 3d^{6.5} 4s^1 4p^0$ for iron, $3s^2 3p^6 3d^8 4s^2 4p^0$ for nickel, $1s^1$ for hydrogen, $2s^2 2p^4$ for oxygen, $3s^2 3p^1$ for silicon, $3s^2 3p^4$ for sulfur, and $2s^2 2p^2$ for carbon. The cutoff radii were 1.8 a.u. for iron, 1.7 a.u. for nickel, 0.5 a.u. for hydrogen, 1.4 a.u. for oxygen, 1.6 a.u. for silicon, 1.7 a.u. for sulfur, and 1.3 a.u. for carbon (1 a.u. = 0.529177 Å). Thermal excitation of electrons was taken into account by the Fermi-Dirac distribution. Γ point sampling was used. The cutoff energy for the plane-wave expansion was 30 Ry. Pressure was found to converge within 1 GPa, with respect to the number of atoms in a supercell, k-point sampling, and plane-wave cutoff energy. Uncertainty in pressure in each simulation was less than 0.5 GPa, indicating that the present simulation time was long enough. Calculations have been carried out using the Quantum-ESPRESSO package (http://www.quantum-espresso.org) (Giannozzi et al., 2009) with a modification to use the Nosé-Hoover thermostat (Sun et al., 2014).

3. Results

We fit the third-order Birch-Murnaghan equation of state (EOS) to the calculated isothermal pressure-volume (P-V) relations to obtain isothermal bulk modulus (K_T). Thermal pressure (P_{th}) and total energy (E) are fitted by a quadratic function to calculate Grüneisen parameter, $\gamma_{th} = \frac{V}{C_V}\left(\frac{\partial P_{th}}{\partial T}\right)_V$, where C_V $\left(=\left(\frac{dE}{dT}\right)_V\right)$ is heat capacity at a fixed volume. Then, compressional velocity (V_P), equivalent to bulk sound velocity for liquid, is calculated by $V_P = \sqrt{K_S/\rho}$, where K_S is adiabatic bulk modulus obtained from K_T as $K_S = (1 + \alpha\gamma_{th}T)\, K_T$; α is thermal expansivity, given by $\alpha = \frac{1}{K_T}\left(\frac{\partial P}{\partial T}\right)_V$, ρ represents density, and T is temperature. For pressure and temperature at which the system was not a liquid state during simulations, these quantities were obtained by extrapolation from data collected at higher temperatures. Fig. 1 illustrates ρ and V_P as functions of pressure and temperature for pure iron and binary alloys investigated. The results for pure Fe and Fe-H alloys are from our previous study (Umemoto and Hirose, 2015). The dependence of $V_P(P)$ on temperature is very small at a given pressure for all liquids investigated here. Both bulk modulus (Fig. S1a) and density decreases with increasing temperature, and resultant V_P (P) hardly depends on temperature. When V_P is represented as a function of density, on the other hand, the dependence of V_P (ρ) on temperature is not small (Fig. S1b). It indicates that the Birch's law, an empirical law for solids predicting a linear relation between ρ and V_P, does not hold for liquid pure Fe and liquid alloys considered here.

By interpolating data of the present isothermal calculations at 4,000 K, 5,000 K, 6,000 K, and 7,000 K, we obtain the ρ and V_P of liquid pure Fe_{64} and binary alloys, $Fe_{76}H_{52}$, $Fe_{104}Si_{24}$, $Fe_{100}O_{28}$, $Fe_{100}S_{28}$, and $Fe_{100}C_{28}$, along geotherms (Table S1). The geotherms are obtained by integrating the equation, $\left(\frac{\partial \log T}{\partial \log \rho}\right)_S = \gamma_{th}$ with assumed ICB temperature (T_{ICB}), which corresponds to the liquidus temperature of the outer core liquid at the ICB pressure. 6,000 K should be the upper bound on T_{ICB}, considering the melting temperature of pure Fe that was determined both computationally and experimentally to be 5,500–6,300 K at 330 GPa (Alfé et al., 2002; Alfé, 2009; Anzellini et al., 2013; Sinmyo et al., 2019) and the depression of melting point by impurity elements. On the other hand, the melting temperature of Fe-H is much lower than that of Fe (Sakamaki et al., 2009), and the T_{ICB} could be as low as 4,800 K (Nomura et al., 2014). Therefore we employ 4,800 K for the lower bound on T_{ICB}. Also we use 5,400 K that is often considered the typical T_{ICB} (Hirose et al., 2013).

From Table S1, we estimate the V and V_P of $(Fe, Ni)_X(H, Si, O, S, C)_{1-X}$ along the three geotherms by ideal mixing (Rivers and Carmichael, 1987); $V = \sum_i x_i V_i$, $K_T = \frac{\sum_i x_i V_i}{\sum_i x_i V_i / K_{T,i}}$, $K_S = (1 + \alpha\gamma_{th}T)K_T$, and, where V_i and $K_{T,i}$ are the volume and K_T of each binary alloy. In order to check the validity of such ideal mixing for both volume and velocity, we have calculated the V and V_P of Fe-Si-O-H alloys, $Fe_{87}Si_1O_{12}H_{28}$ and $Fe_{98}Si_{16}O_2H_{12}$, whose Si and O concentrations are close to those proposed for the outer core composition by Siebert et al. (2013) and Fischer et al. (2015), respectively. We also calculated those for liquid $Fe_{94}S_{13}H_{21}$ and $Fe_{88}C_{14}H_{26}$. The results show that differences in V and V_P between the estimates obtained by ideal mixing and by the calculations in ternary or quaternary systems are at most 0.3% and 0.8% in V and V_P, respectively, at relatively low pressures near the CMB condition and tend to be even smaller at higher pressures (Fig. 2). It indicates that the nonideal mixing effect is negligible on both volume and velocity and mixing behavior is more close to ideal one at higher pressures.

Fig. 3 illustrates the effect of each impurity element, Ni, H, Si, O, S, and C, on ρ and V_P at 330 GPa and T_{ICB} = 4,800 K, 5,400 K, and 6,000 K and at 136 GPa and the corresponding CMB temperatures. As expected, higher concentration of each light element gives rise to lower ρ and higher V_P, while nickel has opposite effects. Note that nickel exhibits a certain effect on V_P but affects ρ to a minor extent. Hydrogen shows the smallest effect on the reduction in ρ per at% impurity concentration and is followed by carbon. These results for ρ are consistent with the previous calculations by Badro et al. (2014), although they did not examine the effect of hydrogen. On the other hand, Badro et al. (2014) reported that the increase in V_P per at% impurity concentration is the strongest for silicon followed by carbon and sulfur, while our data show carbon has the largest effect and is followed by silicon.

The radial pair distribution functions ($g_{\alpha\beta}$) for binary liquid alloys are shown in Fig. 4. Since Fe-Fe peak positions are close to each other between different alloys, the effect of light element on ρ should be stronger when it substitutes Fe atom rather than oc-

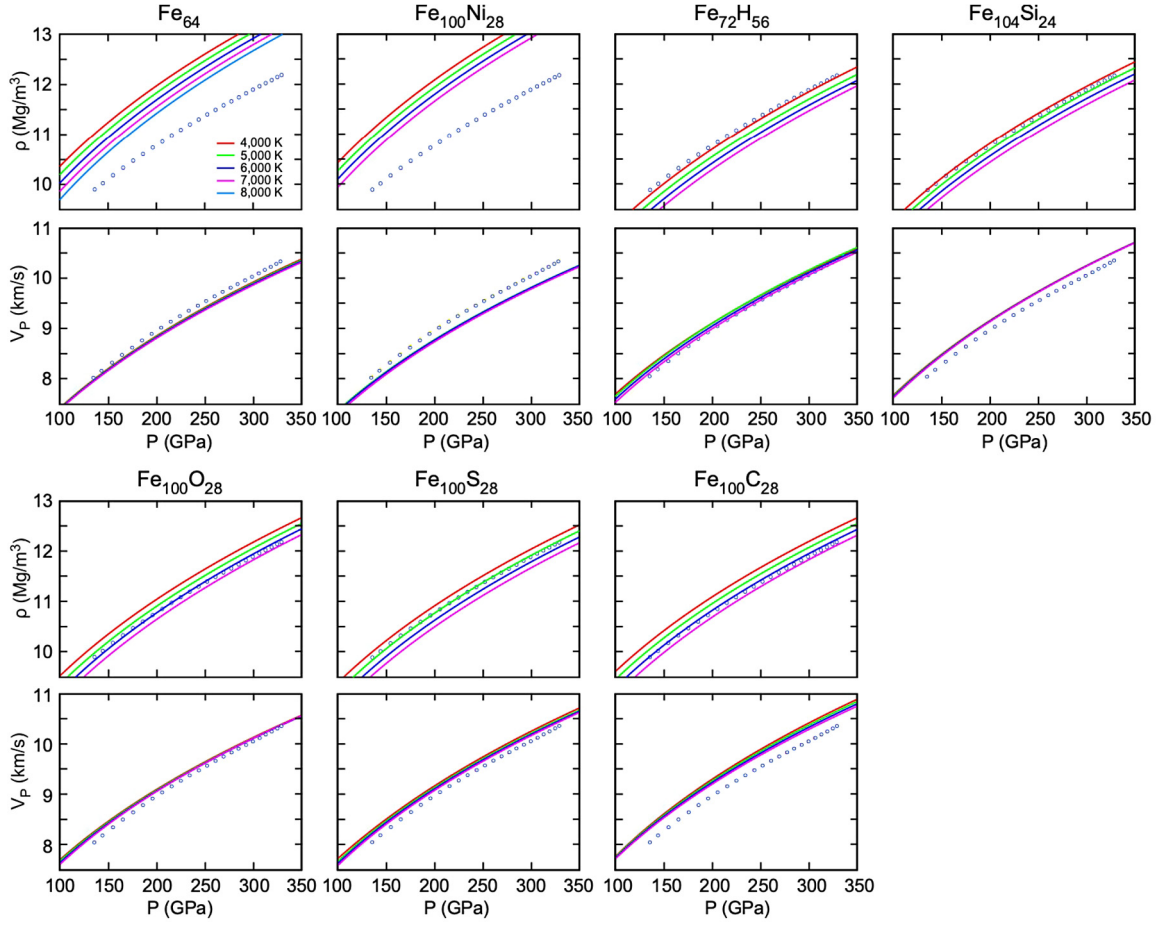

Fig. 1. Densities and bulk sound velocities calculated at 4,000–7,000 K for pure Fe and binary alloys. White circles denote those of the PREM model. Pressure is not adjusted. (For interpretation of the colors in the figure(s), the reader is referred to the web version of this article.)

cupies interstitial sites. In the Fe-Si alloy, being similar to the case of the Fe-Ni alloy, the peak positions of Fe-Fe, Si-Si, and Fe-Si are almost identical to each other, suggesting that incorporation of Si atoms in liquid Fe is substitutional. On the other hand, in the Fe-H alloy, the Fe-H peak position is located at much smaller radial distance and g_{HH} does not show a clear peak, implying that H atoms are distributed almost randomly among Fe atoms and incorporation of H atoms in liquid Fe is interstitial. A greater deviation of the Fe-X peak position from the Fe-Fe one indicates a stronger interstitial character, leading to a smaller effect on ρ per a given atomic concentration.

Fig. 5 compares our calculated density of pure Fe with previous calculations (Ichikawa et al., 2014; Badro et al., 2014) and experiments (Brown and McQueen, 1986; Anderson and Ahrens, 1994). At all pressures, our densities calculated are higher than those by the earlier calculations, while the present compression curves are nearly parallel to those of Ichikawa et al. (2014); their calculations performed at ∼1,000 K lower temperatures are consistent with ours. Our curves show good agreement with the shock-wave compression data by Brown and McQueen (1986) and the EOS parameterized by Anderson and Ahrens (1994) using their data at higher pressures, while there is considerable difference between ours and Anderson and Ahrens's EOS at lower pressures (below ∼250 GPa). On the other hand, the curves obtained by Ichikawa et al. (2014) show smaller deviations from Anderson and Ahrens's than ours at relatively low pressures, but disagreement becomes greater at higher pressure. Since the other previous calculations (Vočadlo et al., 2003; Wagle and Steinle-Neumann, 2019) also showed some deviations from experimental compression curves, these deviations may be intrinsic to DFT-GGA-based FPMD simulations; a better XC functional could address this issue in the future. In order to constrain the chemical composition of the outer core by comparing calculation and seismic observation, we apply pressure correction to reproduce experimental results. To do this, we introduce a pressure adjustment, ΔP_{AA}; $\Delta P_{AA}(P_{calc}, T) = P_{AA}(\rho,T) - P_{calc}(\rho, T)$, where P_{AA} and P_{calc} are pressures on Anderson-Ahrens's and our calculated compression curves at ρ and T. The ΔP_{AA} strongly depends on pressure and temperature; it decreases with pressure and increases with temperature (Fig. 5, inset). Hereafter, we apply pressure adjustment by replacing P_{calc} with $P_{calc} + \Delta P_{AA}$.

4. Discussion

Now we have ingredients to constrain the chemical composition of the outer core. We searched for the possible range of the liquid core composition in Fe + Ni + three different light elements, which accounts for both ρ and V_P in the PREM model, when considering ±1 GPa for pressure, ±0.3% for ρ, and ±0.8% for V_P for errors in the present calculations and the 2σ uncertainties in ρ and V_P in seismological observations given in Masters and Gubbins (2003). Fig. 6 shows the range of possible outer core compositions at each T_{ICB}. Here we assume Fe/Ni = 16 (weight basis), based on the Fe/Ni ratios in chondritic meteorites and in the mantle (McDonough and Sun, 1995).

All candidates except carbon could be a single light element in the core. When T_{ICB} = 6,000 K, the maximum concentration of each light element compatible with the density and velocity of the outer core is 0.89 wt% (33.2 at%) H, 7.6–7.9 wt% (22.4–23.1 at%)

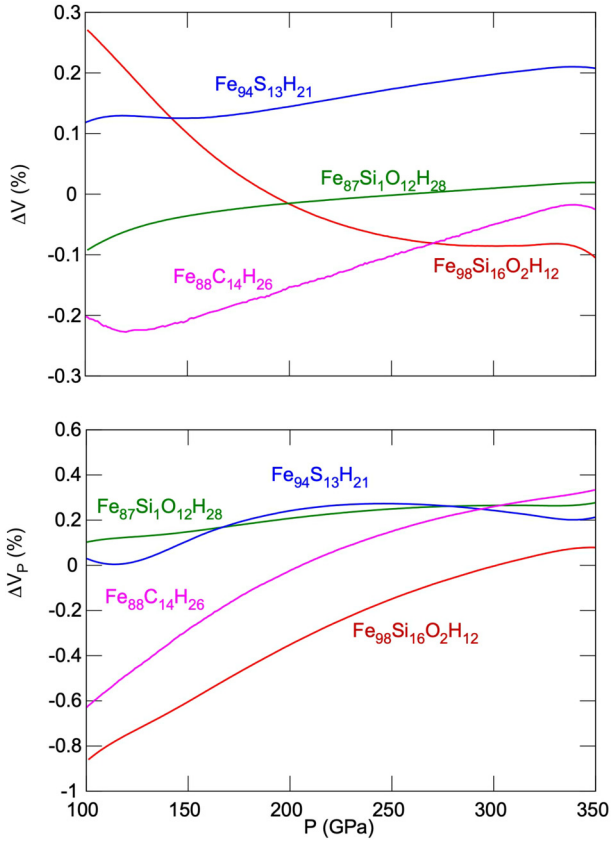

Fig. 2. Difference in volume (ΔV) and bulk sound velocity (ΔV_P) between estimates based on ideal mixing of those of end-members and calculations in ternary and quaternary systems. T_{ICB} = 5,400 K. Pressure is not adjusted.

O, 8.4–8.7 wt% (15.5–16.0 at%) Si, and 12.0–12.8 wt% (19.3–20.4 at%) S, respectively. As T_{ICB} decreases, the density of pure liquid iron along the geotherm increases, and thus the maximum concentration of each light element increases. With the likely T_{ICB} = 5,400 K, we found 0.96–0.99 wt% (35.0–35.7 at%) H, 8.4–8.9 wt% (24.3–25.4 at%) O, 9.3–9.8 wt% (16.9–17.7 at%) Si, and 13.3–14.4 wt% (20.9–22.7 at%) S. With T_{ICB} = 4,800 K, it is 1.05–1.12 wt% (37.0–38.6 at%) H, 8.9–9.9 wt% (25.5–27.7 at%) O, 10.0–10.4 wt% (18.1–18.8 at%) Si, and 14.3–15.0 wt% (22.6–23.6 at%) S. Contrary to the other light elements, carbon cannot be a single core light element (always requires the other light element). The maximum carbon concentration is found in Fe-C-H and decreases as T_{ICB} decreases; 4.2 wt% (15.2 at%) with 0.26 wt% (10.8 at%) H for T_{ICB} = 6,000 K, 3.3 wt% (11.2 at%) with 0.48 wt% (19.0 at%) H for T_{ICB} = 5,400 K, and 2.6 wt% (8.1 at%) with 0.68 wt% (25.5 at%) H for T_{ICB} = 4,800 K. In addition, we also explored the possible outer core compositions by changing the concentration of nickel; Fe/Ni = 16 (weight basis) in Fig. 6, while Fe/Ni = 10 and no nickel in Fig. S2. With increasing the nickel content, main features do not change, although the possible range becomes larger.

We search for the "best" estimate of the outer core composition that is the most compatible with the PREM; it minimizes $\Delta = \sum_i \left\{ \left(\frac{P_{\rho,calc,i} - P_{PREM,i}}{\Delta P_{\rho,i}} \right)^2 + \left(\frac{P_{V_P,calc,i} - P_{PREM,i}}{\Delta P_{V_P,i}} \right)^2 \right\}$, in which $P_{\rho(V_P),calc,i} - P_{PREM,i}$ is the difference in pressure between the pressure of calculation and that in the PREM model for a given ρ_i (or V_{Pi}), and $\Delta P_{\rho(V_P),i}$ is 2σ uncertainty in pressure in seismological observations (Masters and Gubbins, 2003). First, we optimize the concentrations of all light elements to minimize Δ (Case 1 in Table 1). The "best" estimate strongly depends on T_{ICB}. When T_{ICB} = 6,000 K, it includes oxygen as a primary light element (6.6 wt%, 20.4 at%) with tiny amounts of hydrogen, sulfur, and carbon. As T_{ICB} decreases, hydrogen concentration increases while oxygen decreases. When T_{ICB} = 4,800 K, hydrogen only (1.08 wt%, 35.6 at%) is the "best" estimate. Although silicon and sulfur can be a sole light element compatible with the PREM within errors, their amounts in the "best" estimate are nearly negligible. This is because the effects of silicon and sulfur on sound velocity is stronger than those of hydrogen and oxygen (Fig. 3), leading to a larger difference in sound velocity from the PREM. Therefore, our results suggest that the most preferable light element in the outer core is oxygen for higher T_{ICB} like 6,000 K and hydrogen for lower T_{ICB} (5,400 K–4,800 K). Nevertheless, it is natural to expect some sulfur in the core from geochemical considerations. When sulfur concentration is assumed to be 2.3 wt% (Allègre et al., 1995), the concentrations of oxygen for T_{ICB} = 6,000 K and 5,400 K and hydrogen for T_{ICB} = 4,800 K are reduced (Case 2 in Table 1).

Table 1
Liquid composition (wt%) that gives the smallest deviations in density and velocity from the PREM at T_{ICB} =4,800–6,000 K. Fe/Ni = 16 (weight basis).

Case 1: Concentrations optimized for all light elements							
T_{ICB}	Fe	Ni	H	Si	O	S	C
6000 K	87.3	5.45	0.08	0.0	6.6	0.3	0.3
5400 K	90.4	5.65	0.64	0.3	2.4	0.6	0.0
4800 K	93.1	5.82	1.08	0.0	0.0	0.0	0.0
Case 2: Concentrations optimized for all light elements except sulfur (S = 2.3 wt% fixed)							
T_{ICB}	Fe	Ni	H	Si	O	S	C
6000 K	86.8	5.42	0.12	0.0	5.4	2.3	0.0
5400 K	90.7	5.67	0.76	0.0	0.60	2.3	0.0
4800 K	91.1	5.69	0.90	0.0	0.0	2.3	0.0
Case 3: No hydrogen: concentrations optimized for all the other light elements							
T_{ICB}	Fe	Ni	H	Si	O	S	C
6000 K	86.2	5.39	0	0.0	6.9	1.5	0.0
5400 K	85.9	5.37	0	0.0	8.1	0.6	0.0
4800 K	86.6	5.35	0	0.0	9.0	0.0	0.0

For comparison, the outer core composition that minimizes Δ without hydrogen is searched (Case 3 in Table 1). For all T_{ICB}, oxygen concentration is the highest when hydrogen is absent; a small amount of sulfur is found for T_{ICB} = 6,000 K and 5,400 K. In Fig. 7, the compositions optimized for Cases 1–3 are compared for T_{ICB} = 5,400 K. Indeed, the density and velocity of liquid Fe + 0.76 wt% H + 2.3 wt% S + 0.6 wt% O (Case 2) are almost indistinguishable from those of the "best" estimate Fe + 0.64 wt% H + 2.4 wt% O + Si 0.3 wt% + S 0.6 wt% S (Case 1). Note that the compositions including hydrogen (Cases 1 and 2) show better agreement with the PREM than that without hydrogen (Case 3: Fe + 8.1 wt% O + 0.6 wt% S), especially for V_P.

Our result that oxygen concentration is the highest in the "best" estimate for T_{ICB} = 6,000 K is consistent with the earlier calculations by Badro et al. (2014) who considered T_{ICB} = 6,300 K. Nevertheless, there are several differences between the present study and Badro et al. (2014). Their oxygen concentration is smaller than ours. This may be because their density of pure iron is smaller than that by Anderson and Ahrens (1994) to which our pressure is adjusted (Fig. 5). We found that carbon exhibits the largest effect on V_P, while Badro and others claimed that silicon does. It might lead to a difference that our "best" estimate for T_{ICB} = 6,000 K does not contain silicon (Table 1), while Badro et al.'s best composition is 3.7 wt% O and 1.9 wt% Si. Finally, the most important difference is that Badro et al. (2014) did not take hydrogen into account.

The effect of the pressure adjustment (ΔP_{AA}) is significant. Results without the adjustment is summarized in Supplementary Information. As shown in Fig. S3, without the adjustment, hydrogen is necessary in most of the possible outer core compositions.

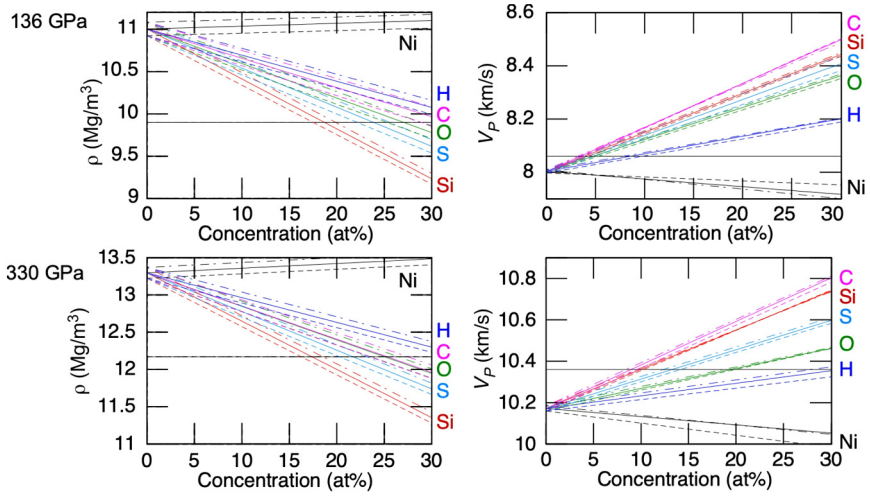

Fig. 3. Changes in density and bulk sound velocity of liquid Fe as a function of impurity concentration (at%) at CMB and ICB conditions. Dashed-dotted, solid, and dashed lines correspond to T_{ICB} = 4,800 K, 5,400 K, and 6,000 K, respectively.

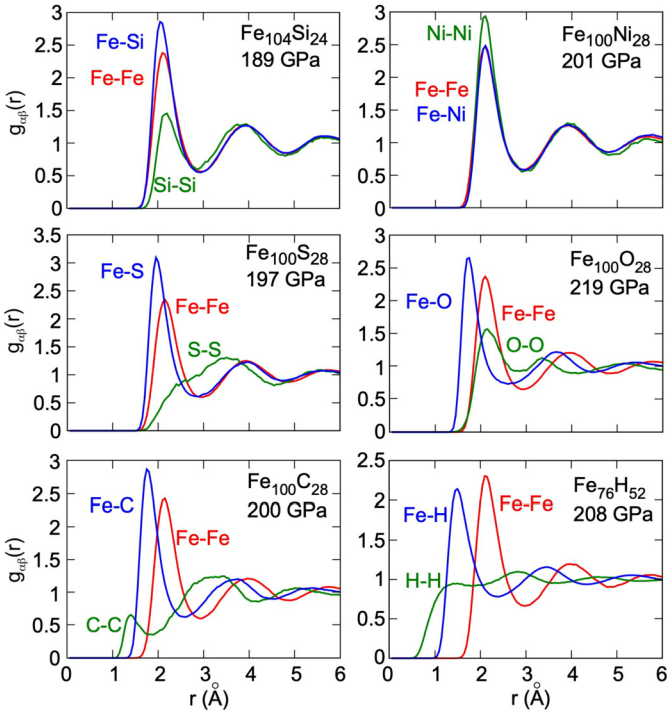

Fig. 4. Radial pair distribution functions ($g_{\alpha\beta}$) for binary alloys at about 200 GPa (pressure is not adjusted).

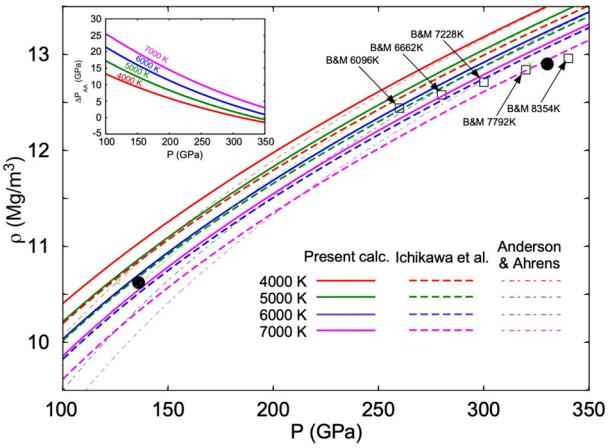

Fig. 5. Calculated isothermal equation of state of pure Fe in this study (solid curve) and by Ichikawa et al. (2014) (dashed curve) at 4,000–7,000 K. They are compared with data by shock experiments (Brown and McQueen, 1986) (squares) and parametrized experimental EOSs (Anderson and Ahrens, 1994) (dashed-dotted line). Black circles represent densities calculated at 136 GPa/4,300 K and 330 GPa/6,300 K by Badro et al. (2014). (inset) The pressure adjustment, ΔP_{AA}.

The "best" estimates without the adjustment are shown in Fig. S4. While the density and sound velocity curves with the adjustment are nearly parallel to the PREM (Fig. 7), those without the adjustment are not. Deviations of calculated ρ and V_{P} in the "best" estimate without the adjustment from the PREM are rather large around the CMB pressure. These deviations around the CMB pressure frequently do not allow liquid iron alloys without hydrogen to reconcile the PREM. As a result, the range of possible outer core compositions without the pressure adjustment is much smaller than that with the adjustment (Fig. S3).

5. Conclusions and future perspectives

We have constrained the range of chemical compositions in (Fe, Ni)$_{\mathrm{X}}$(H, Si, O, S, C)$_{1\text{-}\mathrm{X}}$ that explain the density and velocity of the Earth's outer core by comparing first principles calculations with the PREM model. The liquid iron alloyed with ∼0.8−1.1 wt% H, ∼8−10 wt% O, ∼9−11 wt% Si, or ∼13−15 wt% S is compatible with the observations. The liquid Fe-C does not reconcile the PREM. We searched the "best" estimate which minimizes the deviation of the density and bulk sound velocity from the PREM. Then the most preferable light element has been found to be hydrogen when T_{ICB} = 5,400 K–4,800 K or oxygen when T_{ICB} = 6,000 K. As T_{ICB} decreases, hydrogen and oxygen concentration in the "best" estimate increases and decreases, respectively. For T_{ICB} = 4,800 K, the "best" estimate contains ∼1.1 wt% H solely. If a large amount of hydrogen exists in the outer core, it is likely that hydrogen was incorporated into core metals via chemical reactions with H_2O-bearing silicate melts in a magma ocean (Okuchi, 1997). Although we searched the "best" estimate, it depends on the choice of pressure correction we applied. At present, it is still difficult to specify the chemical composition of the outer core solely based on comparing its density and sound velocity between theoretical calculations and seismological observations.

In addition to the density and sound velocity in the outer core, there are other constraints that narrow down the possible range of the liquid core composition. The simultaneous solubilities of silicon and oxygen in molten iron are limited under core high *P-T* condi-

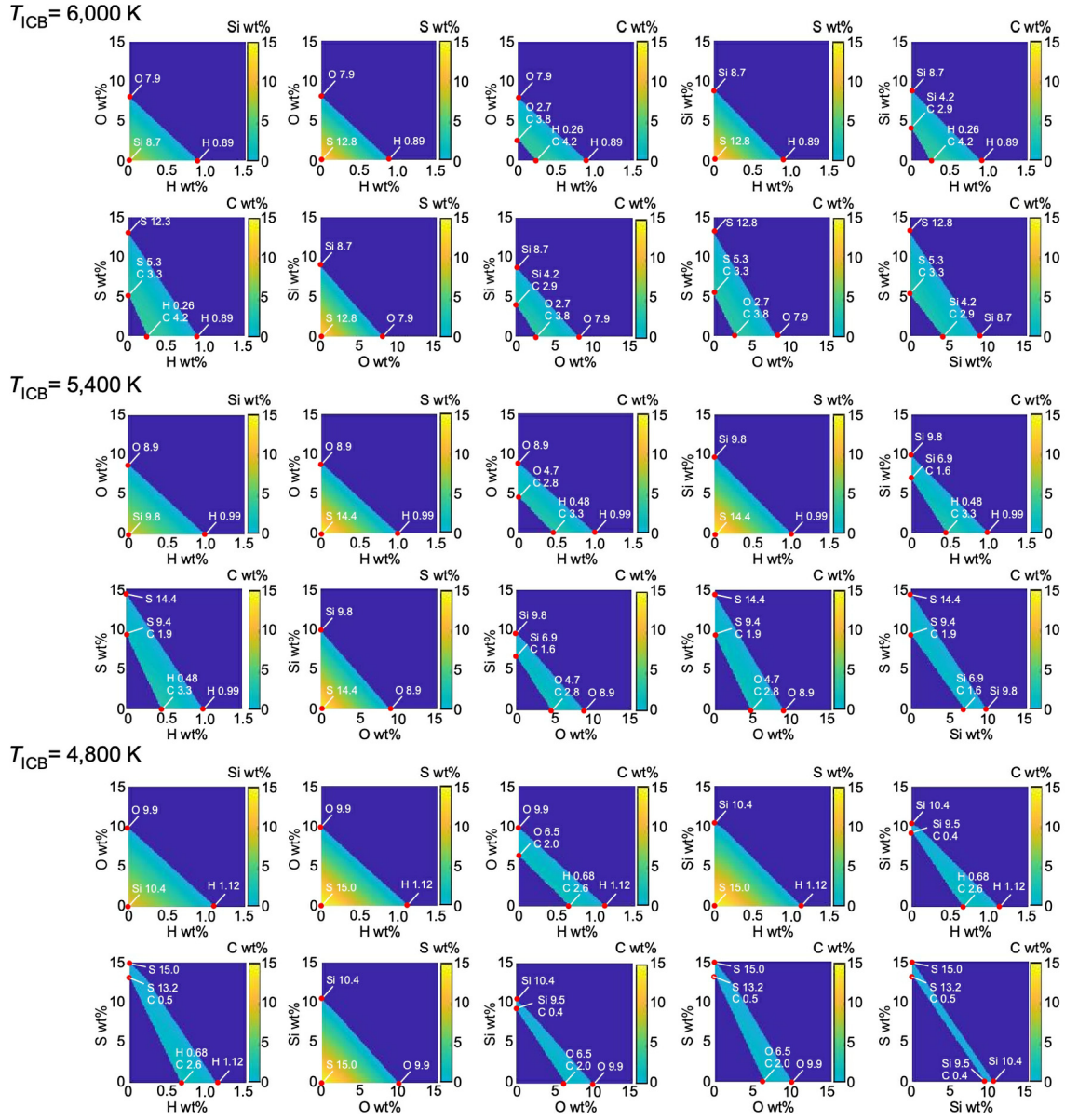

Fig. 6. Possible liquid core compositions of (Fe, Ni)$_X$(X_1, X_2, X_3)$_{1-X}$ that are compatible with the PREM model at T_{ICB} = 4,800–6,000 K. Fe/Ni = 16 (weight basis).

tions (Hirose et al., 2017) as well as at 1 bar (O'Neill et al., 1998). Similarly, it was reported that simultaneous solubilities of hydrogen and carbon in liquid iron is also limited (Hirose et al., 2019). The core compositions with high concentrations of both silicon and oxygen or both hydrogen and carbon are therefore unlikely. The choice of T_{ICB} is key to the estimate of the possible liquid core compositions, as we have seen in the present study. Indeed, the T_{ICB} is uniquely obtained from the outer core composition, since it corresponds to the liquidus temperature of the outer core liquid at 330 GPa. The liquidus temperature of an iron alloy strongly depends on the light element and its concentration. Hydrogen is expected to reduce the melting temperature of iron to a great extent (Sakamaki et al., 2009; Nomura et al., 2014; Hirose et al., 2019). It is supported by the present MD simulations for liquids Fe-H-X studied, although our simulations do not aim for determining the melting temperature precisely. Our results show that hydrogen must be the primary light element in the core when T_{ICB} is not high (~5,400 K–4,800 K), which is consistent with its large effect of depressing the melting temperature of iron. The precise determinations of the liquidus temperatures of iron alloys, both experimentally and computationally, will be the important next step to further constrain the enigmatic outer core composition.

Declaration of competing interest

The authors declare that they have no known competing financial interests or personal relationships that could have appeared to influence the work reported in this paper.

Acknowledgements

We thank Prof. George Helffrich for fruitful discussion. Comments from two reviewers were helpful to improve the manuscript. This work was supported by JSPS Kakenhi (Grant numbers: 26400525, 17K05627, and 16H06285) and MEXT as "Exploratory Challenge on Post-K computer" (Challenge of Basic Science – Exploring Extremes through Multi-Physics and Multi-Scale Simulations). All calculations were performed both at Global Scientific Information and Computing Center and at ELSI, Tokyo Institute of Technology.

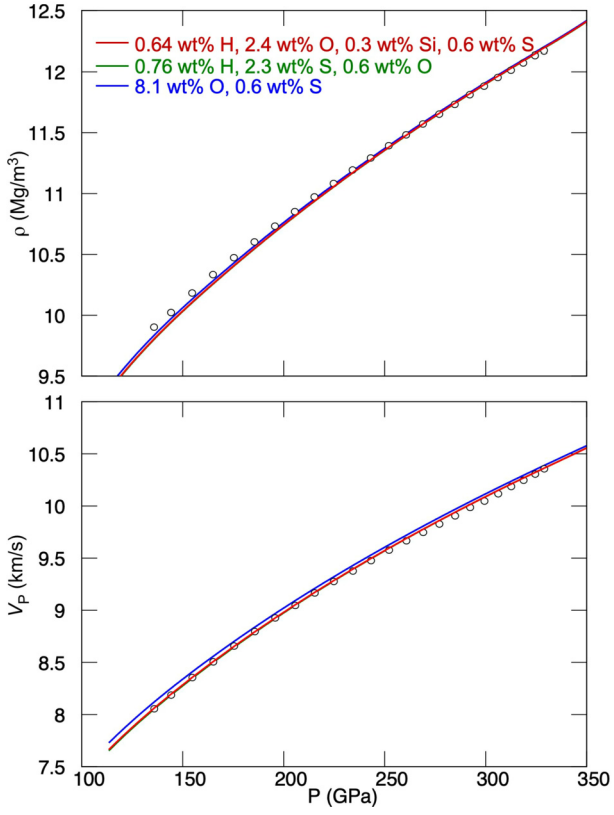

Fig. 7. Density and bulk sound velocity along the geotherm ($T_{\mathrm{ICB}} = 5{,}400$ K) for our "best" estimate of the outer core composition with hydrogen (red: Case 1), with hydrogen and 2.3 wt% S (green: Case 2), and without hydrogen (blue: Case 3). Fe/Ni is assumed to be 16 (weight basis). Circles are from the PREM. Pressure is adjusted by ΔP_{AA}.

Appendix A. Supplementary material

Supplementary material related to this article can be found online at https://doi.org/10.1016/j.epsl.2019.116009.

References

Alfé, D., Price, G.D., Gillan, M.J., 2002. Iron under Earth's core conditions: liquid-state thermodynamics and high-pressure melting curve from ab initio calculations. Phys. Rev. B 65, 165118. https://doi.org/10.1103/PhysRevB.65.165118.

Alfé, D., Gillan, M.J., Price, G.D., 2007. Temperature and composition of the Earth's core. Contemp. Phys. 48, 63–80. https://doi.org/10.1080/00107510701529653.

Alfé, D., 2009. Temperature of the inner-core boundary of the Earth: melting of iron at high pressure from first-principles coexistence simulations. Phys. Rev. B 79, 060101 (R) https://doi.org/10.1103/PhysRevB.79.060101.

Allègre, C.J., Poirier, J.-P., Humler, E., Hofmann, A.W., 1995. The chemical composition of the Earth. Earth Planet. Sci. Lett. 134, 515–526. https://doi.org/10.1016/0012-821X(95)00123-T.

Anderson, W.W., Ahrens, T.J., 1994. An equation of state for liquid iron and implications for the Earth's core. J. Geophys. Res. 99, 4273–4284. https://doi.org/10.1029/93JB03158.

Anzellini, S., Dewaele, A., Mezouar, M., Loubeyre, P., Morard, G., 2013. Melting of iron at Earth's inner core boundary based on fast X-ray diffraction. Science 340, 464–466. https://doi.org/10.1126/science.1233514.

Badro, J., Coté, A.S., Brodholt, J.P., 2014. A seismologically consistent compositional model of Earth's core. Proc. Natl. Acad. Sci. 111, 7542–7545. https://doi.org/10.1073/pnas.1316708111.

Brown, J.M., McQueen, R.G., 1986. Phase transitions, Grüneisen parameter, and elasticity for shocked iron between 77 GPa and 400 GPa. J. Geophys. Res. 91, 7485–7494. https://doi.org/10.1029/JB091iB07p07485.

Clesi, V., Ali Bouhifd, M., Bolfan-Casanova, N., Manthilake, G., Schiavi, F., Raepsaet, C., Bureau, H., Khodja, H., Andrault, D., 2018. Low hydrogen contents in the cores of terrestrial planets. Sci. Adv. 4, e1701876. https://doi.org/10.1126/sciadv.1701876.

Dewaele, A., Loubeyre, P., Occelli, F., Mezouar, M., Dorogokupets, P.I., Torrent, M., 2006. Quasihydrostatic equation of state of iron above 2 Mbar. Phys. Rev. Lett. 97, 215504. https://doi.org/10.1103/PhysRevLett.97.215504.

Dziewonski, A.M., Anderson, D.L., 1981. Preliminary reference Earth model. Phys. Earth Planet. Inter. 25, 297–356. https://doi.org/10.1016/0031-9201(81)90046-7.

Fischer, R.A., Nakajima, Y., Campbell, A.J., Frost, D.J., Harries, D., Langenhorst, F., Miyajima, N., Pollok, K., Rubie, D.C., 2015. High pressure metal–silicate partitioning of Ni, Co, V, Cr, Si, and O. Geochim. Cosmochim. Acta 167, 177–194. https://doi.org/10.1016/j.gca.2015.06.026.

Fukai, Y., Suzuki, T., 1986. Iron-water reaction under high pressure and its implication in the evolution of the Earth. J. Geophys. Res. 91, 9222–9230. https://doi.org/10.1029/JB091iB09p09222.

Giannozzi, P., et al., 2009. Quantum ESPRESSO: a modular and open-source software project for quantum simulations of materials. J. Phys. Condens. Matter 21, 395502. https://doi.org/10.1088/0953-8984/21/39/395502.

Hirose, K., Labrosse, S., Hernlund, J., 2013. Composition and state of the core. Annu. Rev. Earth Planet. Sci. 41, 657–691. https://doi.org/10.1146/annurev-earth-050212-124007.

Hirose, K., Morard, G., Sinmyo, R., Umemoto, K., Hernlund, J., Helffrich, G., Labrosse, S., 2017. Crystallization of silicon dioxide and compositional evolution of the Earth's core. Nature 543, 99–102. https://doi.org/10.1038/nature21367.

Hirose, K., Tagawa, S., Kuwayama, Y., Sinmyo, R., Morard, G., Ohishi, Y., Genda, H., 2019. Hydrogen limits carbon in liquid iron. Geophys. Res. Lett. 46, 5190–5197. https://doi.org/10.1029/2019GL082591.

Hoover, W.G., 1985. Canonical dynamics: equilibrium phase-space distributions. Phys. Rev. A 31, 1695–1697. https://doi.org/10.1103/PhysRevA.31.1695.

Ichikawa, H., Tsuchiya, T., Tange, Y., 2014. The P-V-T equation of state and thermodynamic properties of liquid iron. J. Geophys. Res., Solid Earth 119, 240–252. https://doi.org/10.1002/2013JB010732.

Iizuka-Oku, R., Yagi, T., Gotou, H., Okuchi, T., Hattori, T., Sano-Furukawa, A., 2017. Hydrogenation of iron in the early stage of Earth's evolution. Nat. Commun. 8, 14096. https://doi.org/10.1038/ncomms14096.

Kawaguchi, S.I., Nakajima, Y., Hirose, K., Komabayashi, T., Ozawa, H., Tateno, S., Kuwayama, Y., Tsutsui, S., Baron, A.Q.R., 2017. Sound velocity of liquid Fe-Ni-S at high pressure. J. Geophys. Res., Solid Earth 122, 3624–3634. https://doi.org/10.1002/2016JB013609.

Li, J., Fei, Y., 2014. Experimental constraints on core composition. In: Holland, H.D., Turekian, K.K. (Eds.), Treatise on Geochemistry, vol. 3, second ed. Elsevier, Amsterdam, pp. 527–557.

Malavergne, V., Bureau, H., Raepsaet, C., Gaillard, F., Poncet, M., Surblé, S., Sifré, D., Shcheka, S., Fourdrin, C., Deldicque, D., Khodja, H., 2019. Experimental constraints on the fate of H and C during planetary core-mantle differentiation. Implications for the Earth. Icarus 321, 473–485. https://doi.org/10.1016/j.icarus.2018.11.027.

Masters, G., Gubbins, D., 2003. On the resolution of density within the Earth. Phys. Earth Planet. Inter. 140, 159–167. https://doi.org/10.1016/j.pepi.2003.07.008.

McDonough, W.F., Sun, S.-s, 1995. The composition of the Earth. Chem. Geol. 120, 223–253. https://doi.org/10.1016/0009-2541(94)00140-4.

Morard, G., Siebert, J., Andrault, D., Guignot, N., Garbarino, G., Guyot, F., Antonangeli, D., 2013. The Earth's core composition from high pressure density measurements of liquid iron alloys. Earth Planet. Sci. Lett. 373, 169–178. https://doi.org/10.1016/j.epsl.2013.04.040.

Morard, G., Nakajima, Y., Andrault, D., Antonangeli, D., Auzende, A.L., Boulard, E., Cervera, S., Clark, A.N., Lord, O.T., Siebert, J., Svitlyk, V., Garbarino, G., Mezouar, M., 2017. Structure and density of Fe-C liquid alloys under high pressure. J. Geophys. Res., Solid Earth 122, 7813–7823. https://doi.org/10.1002/2017JB014779.

Nakajima, Y., Imada, S., Hirose, K., Komabayashi, T., Ozawa, H., Tateno, S., Tsutsui, S., Kuwayama, Y., Baron, A.Q.R., 2015. Carbon-depleted outer core revealed by sound velocity measurements of liquid iron–carbon alloy. Nat. Commun. 6, 8942. https://doi.org/10.1038/ncomms9942.

Nomura, R., Hirose, K., Uesugi, K., Ohishi, Y., Tsuchiyama, A., Miyake, A., Ueno, Y., 2014. Low core-mantle boundary temperature inferred from the solidus of pyrolite. Science 31, 522–525. https://doi.org/10.1126/science.1248186.

Nosé, S., 1984. A unified formulation of the constant temperature molecular dynamics methods. J. Chem. Phys. 81, 511–519. https://doi.org/10.1063/1.447334.

Okuchi, T., 1997. Hydrogen partitioning into molten iron at high pressure: implications for Earth's core. Science 278, 1781–1784. https://doi.org/10.1126/science.278.5344.1781.

O'Neill, H.S.C., Canil, D., Rubie, D.C., 1998. Oxide-metal equilibria to 2500°C and 25 GPa: implications for core formation and the light component in the Earth's core. J. Geophys. Res. 103 (B6), 12239–12260. https://doi.org/10.1029/97JB02601.

Pépin, C.M., Dewaele, A., Geneste, G., Loubeyre, P., 2014. New iron hydrides under high pressure. Phys. Rev. Lett. 113, 265504. https://doi.org/10.1103/PhysRevLett.113.265504.

Perdew, J.P., Burke, K., Ernzerhof, M., 1996. Generalized gradient approximation made simple. Phys. Rev. Lett. 77, 3865. https://doi.org/10.1103/PhysRevLett.77.3865.

Poirier, J.P., 1994. Light elements in the Earths outer core: a critical review. Phys. Earth Planet. Inter. 85, 319–337. https://doi.org/10.1016/0031-9201(94)90120-1.

Rivers, M.L., Carmichael, I.S.E., 1987. Ultrasonic studies of silicate melts. J. Geophys. Res. 92, 9247–9270.

Sakamaki, K., Takahashi, E., Nakajima, Y., Nishihara, Y., Funakoshi, K., Suzuki, T., Fukai, Y., 2009. Melting phase relation of FeH_x up to 20 GPa: implication for the

temperature of the Earth's core. Phys. Earth Planet. Inter. 174, 192–201. https://doi.org/10.1016/j.pepi.2008.05.017.

Sato, T., Okuzumi, S., Ida, S., 2016. On the water delivery to terrestrial embryos by ice pebble accretion. Astron. Astrophys. 589, A15. https://doi.org/10.1051/0004-6361/201527069.

Shibazaki, Y., Ohtani, E., Terasaki, H., Suzuki, A., Funakoshi, K., 2009. Hydrogen partitioning between iron and ringwoodite: implications for water transport into the Martian core. Earth Planet. Sci. Lett. 287, 463–470. https://doi.org/10.1016/j.epsl.2009.08.034.

Siebert, J., Badro, J., Antonangeli, D., Ryerson, F.J., 2013. Terrestrial accretion under oxidizing conditions. Science 339, 1194–1197. https://doi.org/10.1126/science.1227923.

Sinmyo, R., Hirose, K., Ohishi, Y., 2019. Melting curve of iron to 290 GPa determined in a resistance-heated diamond-anvil cell. Earth Planet. Sci. Lett. 510, 45–52. https://doi.org/10.1016/j.epsl.2019.01.006.

Sun, T., Zhang, D.B., Wentzcovitch, R.M., 2014. Dynamic stabilization of cubic $CaSiO_3$ perovskite at high temperatures and pressures from ab initio molecular dynamics. Phys. Rev. B 89, 094109. https://doi.org/10.1103/PhysRevB.89.094109.

Umemoto, K., Hirose, K., Imada, S., Nakajima, Y., Komabayashi, T., Tsutsui, S., Baron, A.Q.R., 2014. Liquid iron-sulfur alloys at outer core conditions by first-principles calculations. Geophys. Res. Lett. 41. https://doi.org/10.1002/2014GL061233.

Umemoto, K., Hirose, K., 2015. Liquid iron-hydrogen alloys at outer core conditions by first-principles calculations. Geophys. Res. Lett. 42, 7513–7520. https://doi.org/10.1002/2015GL065899.

Vanderbilt, D., 1990. Soft self-consistent pseudopotentials in a generalized eigenvalue formalism. Phys. Rev. B 41, R7892. https://doi.org/10.1103/PhysRevB.41.7892.

Vočadlo, L., Alfé, D., Gillan, M.J., Price, G.D., 2003. The properties of iron under core conditions from first principles calculations. Phys. Earth Planet. Inter. 140, 101–125. https://doi.org/10.1016/j.pepi.2003.08.001.

Wagle, F., Steinle-Neumann, G., 2019. Liquid iron equation of state to the terapascal regime from ab initio simulations. J. Geophys. Res. 124, 3350–3364. https://doi.org/10.1029/2018JB016994.

Walsh, K.J., Morbidelli, A., Raymond, S.N., O'Brien, D.P., Mandell, A.M., 2011. A low mass for Mars from Jupiter's early gas-driven migration. Nature 475, 206–209. https://doi.org/10.1038/nature10201.